Seismic Design of Flared Columns

David Sanders[1], Hisham Nada[2], M. Saiid Saiidi[1], Khaled Moustafa[3], Suhas Chandane[4], Saad El-Azazy[5]

1) University of Nevada, Reno, Nevada
2) New University Campus Dept., Dammam, KSA
3) Saiful/Bouquet Structural Engineers, Pasadena, CA
4) Martin and Peltyn, Las Vegas, NV
5) California Department of Transportation, Sacramento, CA

INTRODUCTION

Columns with flared tops have been used extensively in California. During the 1994 Northridge Earthquake, these columns performed poorly. In the column designs, it was assumed that lightly reinforced flares, which were not connected to the cap beam, would not be active during an earthquake; this turned out not to be true. The flares did participate and the plastic hinges were forced down into the column effectively shortening the column and causing a large increase in shear. This resulted in brittle failures. Therefore, it was necessary to take steps to isolate the flares from the rest of the column. This has been done by adding a horizontal gap at the top of the flare and a vertical gap between the core of the column and the flare, see Fig. 1.

Five 1/5th scale flared column bents have been tested at the University of Nevada Reno (2,4,5). Two of them had flexure dominated columns with horizontal gaps (LFCD1 and LFCD2), one had flexure dominated columns with horizontal and vertical gaps (LFCD3), and two had shear dominated columns with horizontal gaps (SFCD2 and SFCD3). The flexure-shear ratio was changed by using two different column heights. The flexure dominated columns had a clear height of 64 inches while the shear dominated columns had a height of 37 inches. The columns were pinned at the base with two-way hinges. One tall specimen had transverse flare reinforcement as defined in the Caltrans recommendations (1) (LFCD1) and the others had only minimum transverse reinforcement throughout the flare height (LFCD2, LFCD3, SFCD2, SFCD3) (see Table 1). The two shear dominated specimens had the minimum transverse reinforcement throughout the flare but the gap size in SFCD3 was twice that used in SFCD2. LFCD3 had the same basic details as LFCD2 except that it also had a vertical gap and the size of the horizontal gap was the same as in SFCD3.

BASIC DESIGN

A survey was made on existing bridges in California to develop a prototype. The vertical axial load acting on each column was 0.07 $f'_c A_g$ where A_g is the column cross section and f'_c is the concrete compressive strength. This level resulted in a total axial load of 95 kips. In order to distribute this load along the length of the bent, lead buckets in combination with small hydraulic rams were used. All reinforcement was Grade 60 steel.

The Caltrans recommendations for flares are as follows:

- Minimum gap thickness 2 in. or higher if analysis proved gap closure,
- Nominal longitudinal flare reinforcement, and
- Variable confinement steel ratios.
  ρ_h = 0.45%±0.05, top 1/3 of flare
  ρ_h = 0.075%±0.025, bottom 2/3 of flare
  $\rho_h = 2\ A_b / s\ D$

Where, ρ_h = Confinement steel ratio, A_b = Area of reinforcement bar, s = Spacing of the reinforcement, and D = Diameter of the section.

However, if significant relative rotation between the cap and the column is expected, then the required gap to accommodate this rotation should be calculated and provided. The longitudinal flare reinforcement is just enough to hold the flared part intact. Spacing between longitudinal flare reinforcement shall not exceed 18 in. and not be less than 6 in.

Caltrans procedure was used to estimate whether the gap would close (1). The procedure is based on curvature analysis of the section. Using the effective yield curvature value and the ultimate curvature value, the yield rotation and plastic rotation at the top section of the flare can be calculated. The yield rotation, θ_y, is calculated using the moment-area method by integrating the moment along the column height. For the plastic rotation, θ_p, equation 1 is used.

$$\theta_p = L_p\ (\ \phi_u - \phi_y\ ) \qquad (1)$$

Where L_p = Plastic hinge length, ϕ_y= Effective yield curvature, and ϕ_u= Ultimate yield curvature. The value of the plastic hinge length is calculated using equation 2 provided by Caltrans.

$$L_p = G + 0.3\ f_{ye}\ d_{bl} \qquad (2)$$

Where G = Gap width, f_{ye}= Expected yield stress for longitudinal reinforcement, and d_{bl} = Bar diameter for longitudinal reinforcement. The total vertical displacement of the flare edge can be calculated by multiplying the total rotation, which is the summation of θ_p and θ_y, by the distance from the neutral axis of the section at the ultimate curvature to the edge of the flare. The gap is predicted not to close as long as the calculated deformation is less than the gap width.

For the current specimens, the required gap width was calculated to be 0.372 in. The gap width was set at 0.375 in. for the initial specimens; this was 2 inches in the prototype. The width was doubled for SFCD3 and LFCD3. Finite element analyses done by Nada et al.(5) showed that even the specimens with a gap width of 1.0 in. closes but at a displacement ductility of 10, which is much higher than required.

In the case of LFCD3, vertical gaps were also included on each side of the column core at the top of the column. The gaps were 0.375 in. thick. In the south column, the length of the gap along the column was 6 inches, while in the north column the length was 12 inches. This was done to study the difference in behavior. The south direction was the predominate direction of motion.

To investigate the flare provisions and their effectiveness, two flare details were used. The first detail had flare lateral reinforcement ratio that complied with the Caltrans provisions. The second detail had constant lateral flare reinforcement ratio along the total height of the flare. This was set to the lowest value of ρ_h=0.075% (See Table 1 and Fig. 2).

The bent beam was designed to have a capacity of 1.2 times the capacity of the plastic hinge in the column. This is done to assure that a plastic hinge would form in the columns rather than the beam assuming the gap did not close.

SEISMIC ANALYSIS

Seismic analysis was done using a program called RCSHAKE (3) that was developed at the University of Nevada, Reno. This analysis was used to excite the model with different earthquake records. The program uses an idealized bilinear load-deflection curve. The system was idealized as a single degree of freedom system and the Q-Hyst model was used for the hysteretic properties of concrete. The earthquake time step was scaled with a factor equal to the square root of the model scaling factor to enable the same seismic response of the model as the prototype subjected to the same earthquake. The acceleration level of the earthquake was multiplied by a factor until the response reached the predicted maximum displacement. After the initial scaling, the duration of the earthquake was not changed. The 1994 Sylmar record from the Northridge Earthquake was found to be the most suitable earthquake to fail the tall specimens. Table 2 shows the earthquake motions that were used. The 1994 Northridge Sylmar record was used for all the specimens in order to have a basis for comparison. The peak acceleration for the Northridge Sylmar record is 0.61g. The earthquakes were applied in increasing magnitudes as factor of the base record: 0.15, 0.5… in increments of 0.25 up to 4.0 times Sylmar.

TEST SETUP

The test setup on the shake table consisted of both mass on the specimen and mass off the specimen connected with a rigid link. The mass off the table was placed on what is called the "mass rig", see Fig. 3. The mass was placed off the table to limit the total deadweight on the table and to keep the area around the flares and joints viewable during the tests. The maximum vertical load capacity of the shake table under maximum performance is limited to 100 kips. The total axial load for both columns was approximately 95 kips. Forty kips of axial load was applied to the bent using a self-equilibrating loading system (center-hole rams). The self-equilibrating loading system does not provide inertial mass so a separate inertial system, "mass rig", was needed. The mass rig is a steel structure supported by frictionless pins so that it allows the system to move laterally without restraining it. The four center-hole rams were mounted over the two columns. Fifty kips of lead was placed along the beams in lead buckets and the remaining beam and system weight contributed 5 kips. The specimen footing was tied to the shake table using prestressed steel rods to prevent any uplift or sliding during the test.

Over a hundred strain gauges were attached to the reinforcement in the columns, flares and the beam-column connections for each specimen. Besides strain gauges, 34 transducers were used to measure the curvature along the columns height, beam-column connection deformation, in-plane beam horizontal displacements, out-of-plane beam displacements, and the column base sliding. Accelerometers were mounted on the table and on top of the specimen in both the in-plane and out-of-plane directions of the specimen cap beam.

TEST RESULTS

The accumulative load-displacement curves are shown in Fig. 4. The load-displacement envelopes are also shown. The envelopes show a kink in the load-displacement envelope at lateral displacements of approximately 2.65 in., 2.55 in., 1.65 in. and 3.61 in. for LFCD1, LFCD2, SFCD2 and SFCD3 respectively. These kinks are followed by a large increase in the overall stiffness and capacity of the structure. This behavior was due to the flare gap closure. In the case of LFCD3 (vertical gaps included) there is not the distinctive sudden increase in stiffness (see Fig. 4e). There is a slight rise in the north direction and no increase in the south direction except at the very end. Gap closure was not predicted in any of the specimens by current simplified methods. Displacement prediction models underestimate the displacement capacity of members. Under predicting the displacement/rotation capacity gap region means that the needed gap size is under predicted. Visual evidence of the gap closure was the concrete crushing at the top edge of the flare.

Table 3 summarizes the critical values of displacements and forces. These values were used to calculate displacement ductility ratio based on the effective yield displacement. For each specimen the maximum ductility ratio exceeded the minimum level recommended by Caltrans Seismic Specifications (1). Note that SFCD3 and LFCD3 were the only specimens where the ductility at gap closure was greater than the Caltrans minimum. These are the specimens with the larger horizontal gap.

The moment capacity that was used in designing the cap beam was based on the gap not closing. The maximum measured force was greatly affected by the gap closure. It increased the load by 38 % over the yield first plateau for LFCD1, 35 % for LFCD2, 12% (20% with spike at the end of the south run) for LFCD3, 37 % for SFCD2 and 18% for SFCD3. This difference in the maximum calculated force was one of the reasons behind the shear cracks found in the bent cap beam and shear cracks in the columns. In the cases with the large horizontal gaps, the increase was much less. Fig. 4f shows the final cracking patterns for LFCD1. All of the specimens suffered from extensive cracking at the beam-column connection region starting at very low amplitude runs. Extensive shear and flexural cracks were found in the beams after the lead bucket removal. Concrete spalling typically occurred at the base hinge region and at the flare's outside edge. The amount of concrete spalling in the flare region for LFCD2 was higher compared to that occurred in LFCD1 due to the lower confinement ratio of the LFCD2 flare. Another important visual difference was the concrete spalling observed in the middle third of the flare height for LFCD1 which didn't occur for the other two specimens. In the case of LFCD3 with the vertical gaps, cracks began to form along the vertical gaps at 1.0 times Sylmar. Cracking was greater in the column with the longer vertical gap.

For all of the specimens, the reinforcement in the base-hinge started to yield at low level earthquakes, such as 0.5 times Sylmar. The damage and slipping of the base hinge was high for shear dominated specimens SFCD2 and SFCD3. The strain data shows that the column longitudinal reinforcement started to yield at the flare gap below 1.0 times Sylmar. The beam-column connections started to crack as early as 0.5 times Sylmar while beam bottom longitudinal reinforcement started to yield at 0.75 times Sylmar.

ANALYSIS

Three types of analysis were done on these specimens: simplified models using single degree

of freedom models and Q-Hyst hysteretic models, finite element models, and strut-and–tie models. Due to limited space, these methods are not discussed.

CONCLUSIONS

(1) All the specimens showed good displacement ductility but current gap size prediction methods do not estimate gap size well.
(2) In cases when gap closure is allowed, all structural elements should be designed in accordance with the maximum capacity of the system after gap closure.
(3) Very conservative estimates of gap closure should be used in order to prevent gaps from closing or at least delaying gap closure until very large deformations have occurred.
(4) Minimum flare reinforcement should be used to limit the transfer of load into the flare region.
(5) The specimen with vertical gaps performed well but had additional cracking along gap lines at 1.0 times Sylmar. The short gap length were sufficient to provide separation without the additional cracking.

ACKNOWLEDGEMENTS

This research was funded by Caltrans. The authors appreciate Caltrans for this support. The opinions expressed in this report are those of authors and do not necessarily represent the opinions of the sponsor.

REFERENCES

1. California Department of Transportation, "Seismic Design Criteria Version 1.2", Engineering Service Center, Earthquake Engineering Branch, Sacramento, CA, December 2001.
2. Chandane, S., D.H. Sanders, and M.S. Saiidi, "Static and Dynamic Performance of RC Bridge Bents with Architectural-Flared Columns," CCEER Report No. 2003-08, Department of Civil and Environmental Engineering, University of Nevada, Reno, 324 pp..
3. Laplace, P., "User's Manual for RC-Shake", Version 2.0, University of Nevada, Reno; May, 2003.
4. Mostafa, K. D.H. Sanders, and M.S. Saiidi, "Seismic Behavior of R/C Bridge Bents with Architectural-Flared Columns Including both Horizontal and Vertical Gaps," CCEER Report Number 05-10, Department of Civil Engineering, University of Nevada, Reno, Nevada, Report No. CCEER-05-10, February 2005, 127 pp.
5. Nada, H., D.H. Sanders, and M.S. Saiidi, "Seismic Performance of RC Bridge Frames with Architectural-Flared Columns," CCEER Report No. 2003-01, Department of Civil and Environmental Engineering, University of Nevada, Reno, 476 pp.

Table 1: Flare details for LFCD1, LFCD2, SFCD2, and SFCD3

Flare Detail	**LFCD1**	**LFCD2, LFCD3, SFCD2 and SFCD3**
Transverse reinforcement at top 1/3 of flare height	0.192” Dia. @ 1.1”	0.148” Dia. @ 3.8”
Transverse Ratio	0.44%	0.08%
Transverse reinforcement at remaining 2/3 of flare height	0.148” Dia. @ 3.8”	0.148” Dia. @ 3.8”
Transverse Ratio	0.08%	0.08%
Flare Reinforcement	6 Wires – 0.148 in. dia.	6 Wires – 0.148 in. dia
	LFCD1, LFCD2, SFCD2	**SFCD3 and LFCD3**
Horizontal Gap Width	0.375"	0.75”

Table 2: Loading Program

	Motion Times Sylmar													
LFCD 1	0.15	0.5	0.75	1.00	1.25	1.50	1.75	2.00	2.13	1.75-2	1.75-3			
LFCD 2	0.15	0.25	0.5	0.75	1.0	1.25	1.5	1.75	2.0	2.13	1.75-2			
LFCD 3	0.15	0.25	0.5	0.75	1.0	1.25	1.5	1.75	2.0	2.25	2.75			
SFCD 2	0.15	0.25	0.5	0.75	1.0	1.25	1.5	1.75	2.0	2.25	2.5	2.75	3.0	3.25
SFCD 3	0.25	0.50	0.75	1.0	1.5	2.0	2.5	3.0	3.5	4.0				

Table 3: Structural Response

	LFCD1	**LFCD2**	**LFCD3**	**SFCD2**	**SFCD3**
Effective Yield Displacement (in.)	0.92	0.94	0.80	0.40	0.54
Maximum Displacement (in.)	6.50	6.50	6.75	3.70	7.64
Maximum Measured Force (kips)	64.0	60.4	52.5	97.4	97.0
Ductility Ratio	7.1	6.9	8.4	9.1	14.1
Displacement at Gap Closure (in.)	2.65	2.55	4.32	1.65	3.61
Ductility at Gap Closure	2.9	2.7	5.4	4.0	6.7

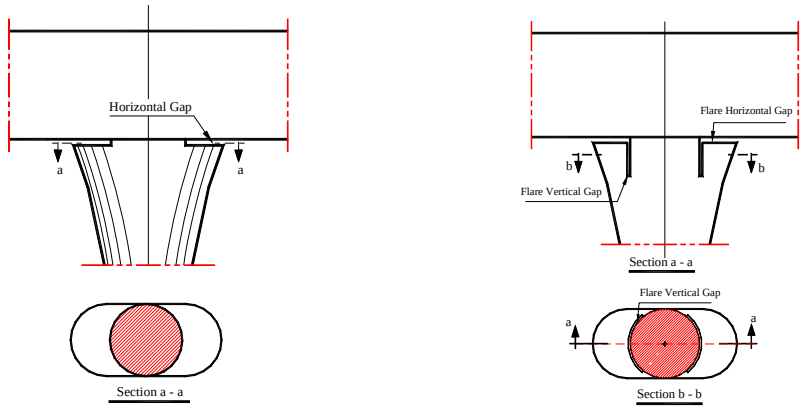

Fig. 1: Layout of Specimens with Horizontal and Vertical Gaps

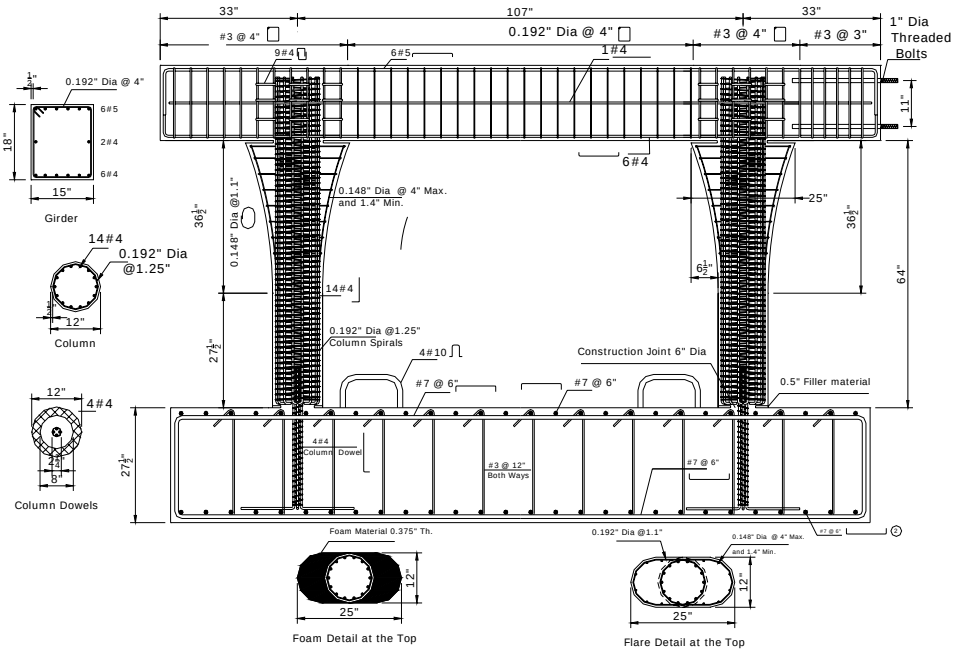

Fig. 2: Reinforcement Details for LFCD2

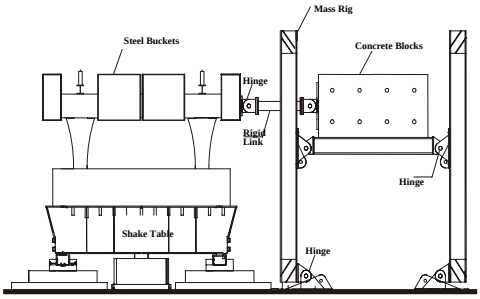

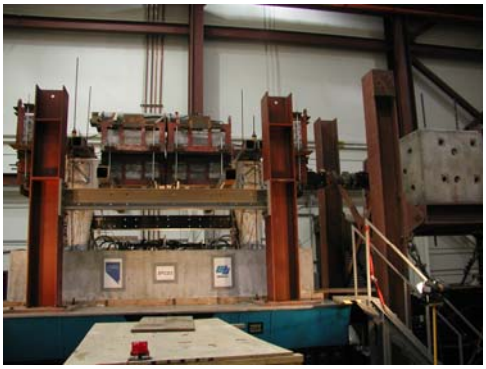

Fig. 3: Shake-Table Test Setup

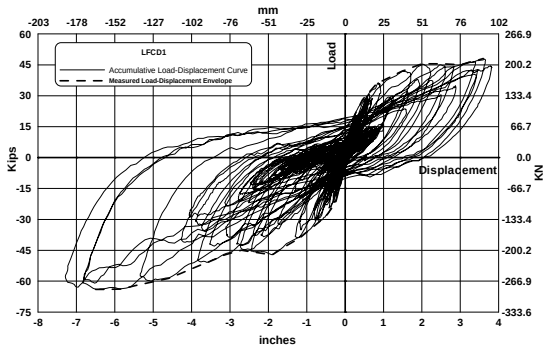

(a) LFCD1

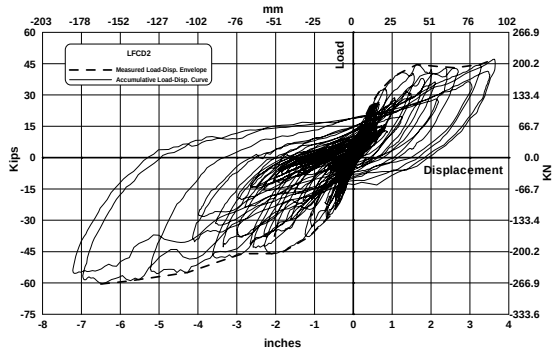

(b) LFCD2

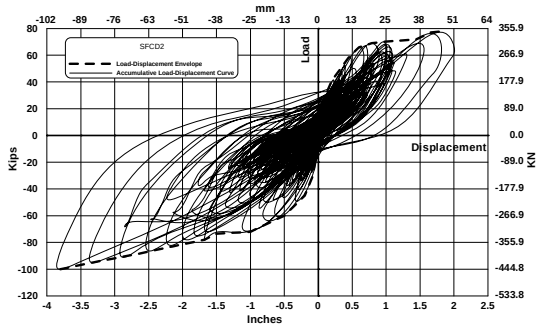

(c) SFCD2

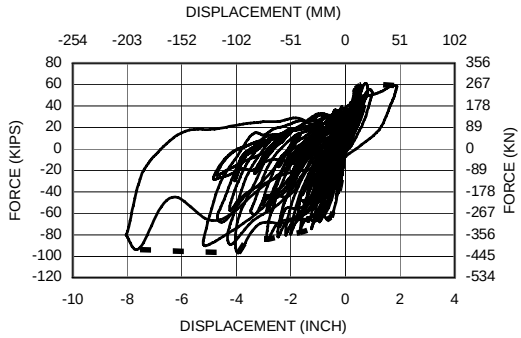

(d) SFCD3

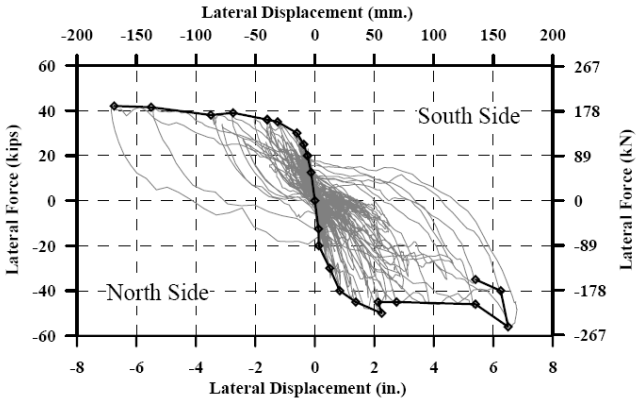

e) LFCD3

f) LFCD1 Final

Fig. 4: Behavior of Specimens